Assessment of Glycerol Gasification: Devolatilization Kinetics and Parametric Analysis

Tala El Samad[1], Idowu Adeyemi[2], Chaouki Ghenai[3], Isam Janajreh[2*]
[1]Department of Engineering, School of Sc. & Tech., City, University of London, London, UK
[2] Mechanical Engineering Department, Khalifa University of Sc. & Tech., Abu Dhabi, UAE
(*Isam.janajreh@ku.ac.ae)
[3]Sustainable and Renewable Energy Engineering Department, University of Sharjah, Sharjah, UAE

Abstract
The forecasted need for diesel fuel continues to rise, and likewise the competitive biodiesel demand in the middle to long term future remains promising. Unfortunately, biodiesel production generates a significant amount of crude glycerol with the byproduct typically exceeding 10% of the biodiesel produced. The current glycerol market cannot accommodate the use of waste crude glycerol; therefore, an alternative solution is needed for the utilization of the crude glycerol and gasification is a potential pathway. In this work, the technical feasibility of gasification of crude glycerol is assessed at two levels, equilibrium modeling which was conducted under ideal conditions, and high-fidelity reactive flow modeling in a tubular reactor. Results revealed that elevated steam ratios are required for the gasification of glycerol to reach high conversion rates of 99% and an acceptable cold gasification efficiency of 40%. Although this value is far off from the conventional coal gasification that hovers around 60%, the anlysis suggests that gasification of crude glycerol can be accepted as an intermediate solution to the expected flood of glycerol generated by the biodiesel transesterification industry before becoming a waste burden.

Keywords: Gasification; Reactive Flow; Devolatilization; Chemical Kinetics; Glycerol Gasification

Nomenclature

ρ	Density	k_{eff}	Thermal conductivity
t	Time	h	Enthalpy
v_x	Axial velocity	Y_i	Mass fraction
v_r	Radial velocity	S_h	External energy source
x	Axial coordinate	S_i	Source term
r	Radial coordinate	$R_{kin,r}$	Arrhenius reaction rate
S_m	Source due to the dispersed/discrete phase interaction	R_i	Addition or the destruction of the species due to the reaction
T	Temperature	D_o	Effective surface area
μ	Dynamic viscosity	$F_D(u-u_p)$	Drag force per unit particle
p	Pressure	u	Fluid phase velocity
F_x	Force in axial direction	u_p	Droplet velocity
F_r	Force in radial direction	g	Gravitational acceleration
E	Internal energy	Re	Reynolds number
$\vec{v}$	Velocity vector	ρ_p	Glycerol droplet density

1. Introduction

Biodiesel is one of the viable alternatives to mitigate global warming and reduce carbon monoxide (CO) emissions that are associated to diesel. It is mainly produced through the transesterification of lipid oil. Crude glycerol is a byproduct of the biodiesel production process, which constitutes nearly 10% by volume of the main product. It contains various adulterants including saponified fatty acids, methanol,

water, catalysts, and ash [1], [2]. Purification of crude glycerol would assist in having a better monetary value; however, the glycerol market is fragile to accommodate this large volume. Albeit the economic feasibility is becoming more promising with increasing government incentives, and the imminent depletion of fossil-based fuel supply. In pure form, glycerol is a simple colorless, odorless sugar alcohol, with low toxicity, high viscosity, and good water miscibility [3]. Moreover, it is characterized with a relatively high heat of calorific value (18 MJ /kg) that makes it a viable source of energy and fuel, which is better than municipal solid waste. There are several routes in using glycerol, but all of these pathways require pre-processing. Purification is the most popular pathway despite the incurred cost and low yield. Although glycerol purification has observed some advancements recently by using electro-dialysis [3] and acidification [4], the associated high treatment cost still creates hindrances for purification methods. As hydrogen resources are on demand, crude glycerol can provide a green source for hydrogen production [5], [6]. In addition to thermochemical conversion, studies investigate biochemical conversion of glycerol to hydrogen biogas through anaerobic digestion. Low hydrogen yield (1.1 < 4) discourages the biological conversion route because there is recovery of only a fraction of the available hydrogen ~26% [6].

The thermochemical glycerol pathway includes pyrolysis, gasification, and reforming as well as combustion of glycerol to give another viable marketing opportunity for it in the energy mix [9]. Combustion of glycerol based on the stoichiometry of Eq.1 is a moderately exothermic reaction but is considered inefficient in comparison to conventional liquid fuels because of its lower calorific value. It also requires a high ignition temperature of 370°C (gasoline is 280°C) and has high viscosity and salt content which promote corrosion and acrolein formation [5].

$$C_3H_8O_3 + 3.5\ (O_2 + \text{with air } 3.57N_2) \rightarrow 3CO_2 + 4H_2O\ (\text{if air} + 3.5 \cdot 3.57N_2) - 1655\ \text{kJ/mol} \quad (1)$$

Alternatively, production of syngas from crude glycerol through gasification by partial combustion at a sub-stoichiometric ratio and using an additional power source can be a viable route. For example, gasification using microwave plasma was attempted by Yoon et al. [5] where they investigated the influence of microwave power, oxidizer in pure form, and steam moderator under different values. Their experimental results revealed direct proportionality between microwave power and the gasification efficiency, and syngas heating value. The oxygen and steam ratios, however, were inversely proportional to the gasification efficiency but with the best reported results at oxygen: glycerol molar ratio between 0–0.4. In another study, Tapah et al. [10] carried out catalytic supercritical water gasification at lower temperatures in the range of 400–550°C and pressures of 170–270 bar; a high yield of syngas as well as volatile hydrocarbons (methane and ethylene) was achieved. Glycerol can be viewed as an oxidated fuel and hence possesses low to zero oxidizing capacity (as for the case of pyrolysis) which can be used thermochemically to produce the desired syngas. Experimental pyrolysis of glycerol in a steam environment with the simplest thermochemical conversion setup was reported by Stein et al. [11], and another attempt by Valliyappan et al. [12] was done at 600°C where the evolved gases were found to consist mainly of CO, CO_2, H_2, CH_4 and C_2H_4. The most effective methods of hydrogen production from glycerol known today are the aqueous or steam-phase reforming that stoichiometry proceeds according to **Error! Reference source not found.** as:

$$C_3H_8O_3 + 3H_2O \rightarrow 3CO_2 + 7H_2 + 128\ \text{kJ/mol} \quad (2)$$

It is a two-step method that involves endothermic pyrolysis as Eq.3 and exothermic water-gas shift according to Eq. 4.

$$C_3H_8O_3 \rightarrow 3CO + 4H_2 + 250\ \text{kJ/mol} \quad (3)$$

$$CO + H_2O \rightarrow CO_2 + H_2 - 41\ \text{kJ/mol} \quad (4)$$

Adhikari et al. [13] suggested a high steam to glycerol molar ratio (H_2O:$C_3H_8O_3$) of 9:1, a temperature beyond 627°C, and atmospheric pressure to ensure the largest hydrogen yield with minimal methane. Lower temperatures were also reported in the presence of catalysis; operating temperatures ranged

between 600°C when using Ru/Y_2O_3 [14] and at 400°C when using Ir/CeO_2 [15]. Other catalysts including Ni/AL_2O_3 and Ni/TiO_2 showed to have different effects by varying temperature [16]. The temperatures, and steam to glycerol ratios are thought to be the most pronounced parameters influencing syngas production. Although there are several studies that have investigated the gasification of glycerol, there are very few studies that have focused on the gasification of crude glycerol with steam and oxygen through entrained flow gasifiers. Moreover, there remains a need for the assessment of the economic feasibility of the gasification process.

In this study, the techno-economic feasibility of glycerol gasification was evaluated. Two different modeling approaches, namely the equilibrium and numerical gasification models were utilized. Equilibrium modeling was conducted under ideal conditions, and high-fidelity reactive flow modeling in a tubular reactor. The properties and behavior of the crude glycerol such as thermogravimetric assessment, calorific value, pour point were determined. Moreover, the parametric analysis with different water to oxidant ratio and temperature were investigated based on the cold gasification efficiency. The economics of the gasification of the crude glycerol was evaluated under varying gasification temperature conditions.

2. Materials and Methods

2.1 Materials

Samples of glycerol byproduct were collected from our laboratory after running several biodiesel transesterification experiments of waste cooking oil. These experiments are conducted near 50°C but at various methanol: triglycerides molar ratios. In addition, catalyst concentration of NaOH or KOH between 0.25% and 1% was used. Other samples obtained from the patented sonicated assisted transesterification, that has faster and higher conversions compared to classical stirring, were also utilized [21]. This latter process typically runs at near stoichiometric ratio of 3:1 and without catalysis. The details of these processes are described in previous works of the authors [22, 23]. Additionally, pure glycerol is purchased from Sigma Aldrich for baseline/ reference analysis and testing. These samples were subjected to several thermal, physical, and thermodynamic properties assessment tests following ASME standards to obtain density via hydrometer, flash point, cloud point, calorific value through Bomb Parr 6100 Calorimeter, and viscosity. Additionally, proximate and ultimate analyses were carried out using Thermogravimetric Analysis (TGA) (STA:600 thermo-scientific) at two distinct heating rates 5°C/min and 2°C/min, followed by 5 elemental analysis (CHNS and O thermo-scientific) analysis using the Flash Analyzer. These tests were carried out in triplicates to establish uncertainty measurements and to reduce statistical errors. The TGA, Flash, and Bomb calorimetry describes the material composition of the crude and pure glycerol.

2.2 Equilibrium-Based Analysis Method

The gasification analyses were carried out at two levels, low and high fidelities. The low fidelity method is an equilibrium-based systematic gasification and is carried out using the evaluated unit glycerol formula inferred from the conducted TGA and elemental analyses. It allows idealistic assessment of the influence of several process parameters including the oxidizer, the moderator as well as temperature. The model is based the assumption of a well stirred plug flow reactor. The gasification is based on "Gibbs Energy" minimization principle of the largest possible compositional species list. This model is designated to estimate the product species and heat required for various conditions based on a zero-dimensional approach. The model in use was developed by Shabbar and Janajreh [24] and assumes an infinite reaction time with no reference to the distribution of species nor the geometric aspects of the reactor. The model also presumes chemical/ thermodynamic equilibrium and does not take reaction chemical kinetics into consideration nor any intrinsic behavior. The basis of the system depends on the Equilibrium Constant Method (ECM) which is used for the determination of species concentration at equilibrium as well as product temperature and pressure [25] to provide the concentration of all possible products. A detailed description of how the model works and what equations it uses can be found elsewhere [24]. Overall, the gasification is prescribed by combined devolatilization, pyrolysis, and gas-shift of the inferred molecular molar formula as per the reaction in Eq 5. The equilibrium process

involves the conversion of the feedstock with water and limited oxidant to various species. The main products include carbon monoxide, carbon dioxide, hydrogen, water and methane.

The performance metrics of gasification are represented by the evaluated conversion of the feedstock, cold gasification efficiency, and the molar fraction of the syngas. A lower cold gasification efficiency implies low feedstock conversion, lower molar fraction of the syngas species, and also lower product calorific values; hence the cold gasification efficiency (CGE) has an extensive usage and is defined as:

$$\mathrm{CGE} = \frac{\sum_{H_2}^{CO} \text{Heating value of syngas}}{\text{Heating value of feedstock}} \tag{6}$$

2.3 Reactive Flow Simulation Method

In the high-fidelity reactive flow simulation of gasification analysis, the assumption of homogenized plug flow reactor is relaxed, and a more realistic three-dimensional tubular reactor is considered using a reduced set of actual reactions and their kinetics. Therefore, spatial and intrinsic/ temporal, variations of the reactive flow are pursued mostly at the exit of the gasifier. Gasification efficiency, generally, is better estimated with reactive flow in comparison to the equilibrium-based analysis. Equilibrium simulation may involve heat losses to the surroundings, as well as turbulence, kinetic and dynamic limitations. The reactor geometry and boundary conditions are those at two concentric centers of the reactor for the injection of the glycerol in the form of droplets at high pressure that lead to atomization which is aided by any co-firing or swirling stream around it. The geometry of the reactor under study is similar to that of a drop tube reactor [32], consisting of 1.5 m long by 0.066 m radius with a thick, resilient stainless-steel wall. The heating is applied at the tube wall via nichrome wires which are included around the ceramic housing of the stainless-steel tube. The domains are discretized via finite volume quadrilateral cells using multi-blocking technology to facilitate meshing, and it comprises of 120,500 cells as baseline and consisting of two zones (interior and wall) as depicted in Fig. 1.

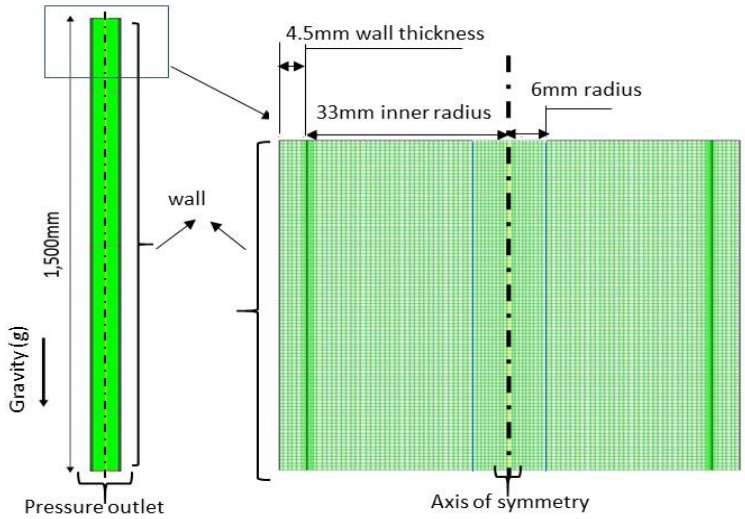

Fig. 1: Topography of reactor and mesh details

Accurate modeling of the gasification phenomenon requires application of the four conservative laws, i.e., mass, momentum, energy and species transport in chemically reacting two-phase flow. The model follows Eulerian-Lagrangian formulation, which accounts for the discrete atomized droplets phase introduced to the gaseous continuous phase in a turbulent flow regime. The turbulence is governed by the common SST k-ω model, the phase gasification via reactive species transport, droplet devolatilization from TGA analysis, droplet dispersion via the Stochastic Discrete Random Walk model, the radiation via (P1 model) and droplet turbulent dispersion using cloud tracking model. The conservation of mass is based on Eq. 7 and the momentum based on Eq. 8 & 9 as:

$$\frac{\partial \rho}{\partial t} + \frac{\partial (\rho v_x)}{\partial t} + \frac{\partial (\rho v_r)}{\partial t} + \frac{\rho v_r}{r} = S_m \tag{7}$$

Where ρ is the density, S_m is the source terms due to the dispersed/discrete phase interaction, t is time, r is for radial position, x is the axial location and v is velocity. The momentum equation is represented as follows:

$$\frac{\partial(\rho v_x)}{\partial t} + \frac{1}{r}\frac{\partial}{\partial x}(r\rho v_x v_x) + \frac{1}{r}\frac{\partial}{\partial r}(r\rho v_r v_x) = -\frac{\partial p}{\partial x} + \frac{1}{r}\frac{\partial}{\partial x}\left[r\mu\left(2\frac{\partial v_x}{\partial x} - \frac{2}{3}(\nabla\cdot\vec{v})\right)\right] + \frac{1}{r}\frac{\partial}{\partial r}\left[r\mu\left(\frac{\partial v_x}{\partial r} + \frac{\partial v_r}{\partial x}\right)\right] + F_x \quad (8)$$

$$\frac{\partial(\rho v_r)}{\partial t} + \frac{1}{r}\frac{\partial}{\partial x}(r\rho v_x v_r) + \frac{1}{r}\frac{\partial}{\partial r}(r\rho v_r v_r) = -\frac{\partial p}{\partial x} + \frac{1}{r}\frac{\partial}{\partial x}[r\mu(\frac{\partial v_x}{\partial r} + \frac{\partial v_r}{\partial x})] + \frac{1}{r}\frac{\partial}{\partial r}\left[r\mu\left(2\frac{\partial v_r}{\partial r} - \frac{2}{3}(\nabla\cdot\vec{v})\right)\right] - 2\mu\frac{v_r}{r^2} + \frac{2}{3}\frac{\mu}{r}(\nabla\cdot\vec{v}) + \rho\frac{{v_z}^2}{r} + F_r \quad (9)$$

Where p is the pressure, μ is the fluid viscosity, and F_x is the present body forces in the form of gravitational force and the divergence of the velocity is expressed per Eq. 10 as:

$$(\nabla\cdot\vec{v}) = \frac{\partial v_x}{\partial x} + \frac{\partial v_r}{\partial r} + \frac{v_r}{r} \quad (10)$$

The conservation of energy is written per Eq. 11 as:

$$\frac{\partial(\rho E)}{\partial t} + \nabla\cdot\left(\vec{v}(\rho E + p)\right) = \nabla\cdot(k_{eff}\nabla T - \sum_j h_j\vec{J}_j + (\bar{\bar{\tau}}_{eff}\cdot\vec{v})) + S_h \quad (11)$$

Where E is the internal energy ($E = h - \frac{p}{\rho} + \frac{v^2}{2}$), h is the enthalpy ($h = \sum_j Y_j h_j$), k_{eff} is the effective conductivity, and Y_i is the mass fraction. The S_{h} is any unaccounted for external energy source. The conservation of species is described as:

$$\frac{\partial(\rho Y_i)}{\partial t} + \nabla\cdot(\rho\vec{v}Y_i) = -\nabla\cdot\vec{J}_i + R_i + S_i \quad (12)$$

Where S_i is the source term while R_{i} is the addition/destruction of the species due to the reaction and is expressed per Eq. 13 as:

$$R_{j,r} = R_{kin,r}(p_n - \frac{R_{j,r}}{D_{0,r}})^N \quad (13$$

Where $R_{\text{kin,r}}$ is the Arrhenius reaction rate and is written per Eq. 14 as:

$$R_{kin,r} = A_r {T_p}^{\beta r} e^{-(E_r/RT_p)} \quad (14)$$

Where D_o is the effective droplet surface area which is a function of the localized temperature and droplet diameter and is written per Eq. 15 as:

$$D_{0,r} = C_{1,r}\frac{[(T_p + T_\infty)/2]^{0.75}}{d_p} \quad (15)$$

The discrete droplet is governed by Lagrangian equation and is written per Eq. 16 as:

$$\frac{du_p}{dt} = F_D(u - u_p) + \frac{g_x(\rho_p - \rho)}{\rho_p} + F_x \quad (16)$$

With $F_D = \frac{18\mu}{\rho_p {d_p}^2}\frac{C_D Re}{24}$ and Re is the droplet *Reynolds* number described as $Re = \frac{\rho d_p|u_p - u|}{\mu}$. The $F_D\ (u - u_p)$ in Eq. 16 is the drag force per unit droplet mass; u is the fluid phase velocity; u_p is the droplet velocity; ρ is the gas phase density while ρ_p is the glycerol droplet density. The numerical model of the gasification processes in an entrained flow gasifier was done with Ansys Fluent. The model

implements Eulerian scheme for the resolution of the conservation of mass, species, momentum and energy in the gas phase while using the Lagrange scheme to obtain glycerol droplet position, velocity and temperature. The following model assumptions were made:
1. The gasification process is steady and isothermal wall temperature was used
2. The injected glycerol droplets are spherical and uniformly distributed
3. There was no char or solid components in the glycerol
4. The gasification pressure is uniform and atmospheric
5. The gasification is based on pyrolysis and volatile reactions

A mesh sensitivity study has been performed by Adeyemi [33] to assess the mesh discretization independency, allowing for the trade-off between refined meshes and computational time. The boundary conditions applied to the model are those at the stipulated inlet prescribed as velocity for each of the glycerol and steam flows at the specified temperature and pressure. The reactor wall is kept at constant temperature mimicking the drop tube reactor which is equipped with three controlled heating elements with a temperature feedback loop that maintains the wall at a fixed temperature. At the outlet, the atmospheric pressure condition is assumed with no vertical gradient to the velocity and other flow variables, attaining a solution without any recirculation for an established and steady flow. The system requires an input of reaction kinetics of glycerol pyrolysis. These devolatilization chemical kinetics are obtained mathematically using an approximation method developed by Lü et al. [26] that are inferred from the TGA mass-conversion curve of glycerol. This conversion is expressed by Eq. 17 as:

$$\frac{dX}{dt} = k(1-X)^n \qquad \text{with } X = \frac{W_o - W_t}{W_o - W_f} \tag{17}$$

Where n is the reaction order, X is the loss in mass fraction (W_o, W_t, and W_f are the initial, current, and final weights respectively from taken from the TGA curve), and k is the Arrhenius rate coefficient. To solve **Error! Reference source not found.**, Lü et al. [26] approximated a solution following Eq. 18 as:

$$\ln(1-X_1) = -\gamma T_1 + \gamma T_o \text{ and } \ln(1-X_i) = \ln(1-X_{i-1}) - \gamma T_i + \gamma T_{i-1} \quad \text{for } i = 1,2,\ldots \tag{18}$$

where γT is expressed as:

$$\gamma T = \frac{A}{\beta}\frac{\frac{RT^2}{E}\exp\left(-\frac{E}{RT}\right)}{1+\frac{2RT}{E}} \tag{19}$$

Where T is the temperature and R is the universal gas constant, β is the heating rate, and A and E are the kinetic parameters. By solving **Error! Reference source not found.** through **Error! Reference source not found.**, values of the activation energy (E) and the pre-exponential factor (A) can be approximated. Using the "lsqnonlin" Matlab function as the least squares fit for non-linear thermogravimetric obtained data [32], a smoother curve can follow the TGA devolatilization as depicted in Fig. 2. The curve fit is shown for two distinct heating rates implemented in the TGA, 5°C/min and 20°C/min. The reaction order value (n) is taken as 0.2 and is based on the work of Adhikari et al. [16]. The obtained kinetic values for each of E and A are 9.9×10^7 J/kgmol and 7.2×10^7 s^{-1}, respectively. These will be used in the devolatilization reaction of the glycerol pyrolysis that proceeds gasification reaction.

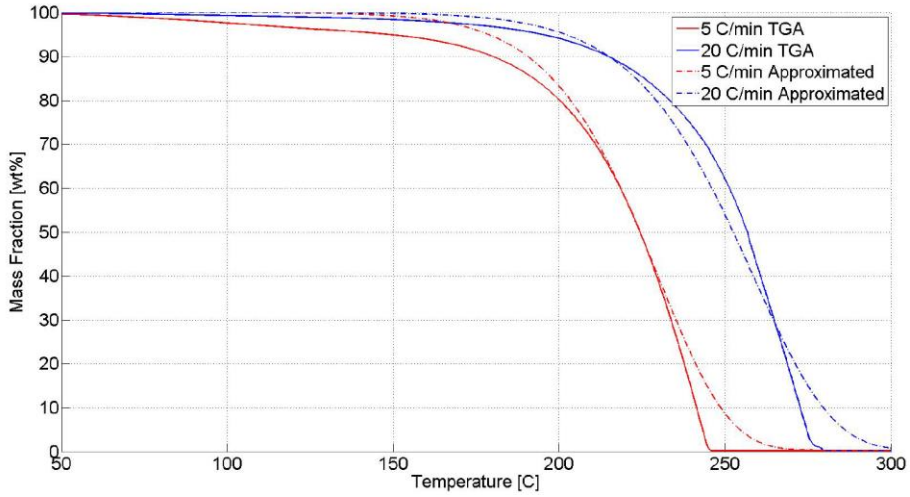

Fig. 2: Approximated devolatilization curve compared to TGA curve of pure glycerol

The gas shift or oxidation reaction kinetics are obtained from the available literature and a reduced set of these reactions is used in a coupled reactor flow with the absence of solid char for liquid feedstock as summarized in Table [27]. Generally, a dedicated research and body of literature build around evaluation of the chemical kinetics for either individual elemental reaction or whole lump-sum reaction as for the case of devolatilization.

Table 1: List of the homogenous reactions and their kinetic used in the high-fidelity model [27]

Reaction	Kinetic parameters A and E
R1: $2CO + O_2 \rightarrow 2CO_2$	A=$10^{17.6}$ m^3 mol^{-1} s^{-1}, E=166.28 MJ $kmol^{-1}$
R2: $2H_2 + O_2 \rightarrow 2H_2O$	A=$1e^{11}$ m^3 mol^{-1} s^{-1}, E=42 MJ $kmol^{-1}$
R3: $CO + H_2O \leftrightarrow CO_2 + H_2$	A=0.0265 m^3 mol^{-1} s^{-1}, E=65.8 MJ $kmol^{-1}$
R4: $2CO + O_2 \rightarrow 2CO_2$	A=7.2x10^7 m^3 mol^{-1} s^{-1}, E=99.0 MJ $kmol^{-1}$

In the remaining part of the manuscript, we analyze the physical and thermal differences between crude and pure glycerol. Furthermore, we detailed and discussed the obtained results of the glycerol gasification following the equilibrium and reactive flow modeling and evaluated and compared their conversion metrics.

3. Results and Discussion

3.1 Glycerol Analysis

Crude glycerol requires expensive refining to match its properties to pure glycerol grade used in pharmaceutical and food products. To emphasize the difference, several samples of the crude and the reference pure glycerol are collected, and their physical and thermal properties are evaluated. The image of the WCO transesterification byproduct glycerol and the Sigma-Aldrich pure is shown in Fig. 2. It clearly depicts the difference of the dark brown opaque crude and the transparent pure. The coloring is attributed to the residues of the transesterification reaction that consist of tri-, di- and mono-glycerol in addition to traces of saponification reaction product, water, and unreacted components that form methoxides in combination with alcohol. Additionally, coloring of the source feedstock can be inherited in both the fatty acid methyl ester and the generated crude glycerol.

Fig. 2: Photos of different TG (Neem, Karanja, Castrol, and Palm) in the back row, and their resulting transesterification crude glycerol in the front row, notice also the photo of Sigma-Aldrich pure glycerol on the top

The heating values (HHV) of the pure and crude glycerol are obtained using the Bomb Parr 6100 Calorimeter. Some variations are obtained in the crude with an average value of 22.95+0.85 MJ/kg while the pure has a mean value of 17.5±0.1 with slight deviation that falls within the calorimeter device error. The larger deviation in the crude glycerol is attributed to several factors, including the feedstock source, variation in pre-treatment, and the degree of reaction completion which depends on the deployed conversion technology, reaction temperature, and reaction time. Three samples were obtained from three different WCO batches, but following nearly similar pre-treatment by using paper filter of 10 mm mesh size, and drying at 100°C overnight for 10 hours. They are also collected from three separate transesterification runs of the continuous sonicated reactor operated under equal power conditions. Thus, the observed variation in the heating value is mainly attributed to any inherited variation in the feedstock and to a lesser degree of the conversion conditions. The densities of the crude and pure glycerol are respectively 1.22±0.25 kg/L and 1.25±0.05 kg/L and were measured by means of a graded hydrometer device between 1.1–1.30 g/mm^3 which would vertically float at the surface of homogenized samples of crude and pure glycerol. Given the accuracy of the calibration of these devices, they are direct and favored over the classical volume-weight measurements. The lower crude density is attributed to the presence of the excess and lighter methanol, although traces of other heavy glycerides as well as the soluble catalyst (KOH or NaOH) are still present. The kinematic viscosity is evaluated by the flowing time method of the standard ASME glass tube, while the dynamic viscosity is inferred by multiplying that by the measured density. Similar to the density, a lower crude glycerol viscosity is measured and is marked 0.52±0.06 Pa·s compared to 0.54±0.02 Pa·s for pure glycerol which is attributed to the remaining soluble methanol fraction. The results along with other measured values for the flash and pure points vapor pressure are listed in Table .

Table 2: Summary of standard tested value for crude and pure glycerol

Test	ASTM Standard	Crude glycerol	Pure glycerol
Flash point	ASTM D93	154°C±3.0	160°C±3.0
Cloud point	ASTM D2500	10.0°C±1.0	12.0°C±1.0
Pure Point	ASTM D97	4.0°C±1.0	7.0°C±1.0
Density	ASTM E100 & ASTM 1298	1.22±0.25 kg/L	1.25±0.05 kg/L
Vapor pressure	ASTM D323	0.003 mmHg	0.003 mmHg
Kinematic Viscosity	ASTM D445 at 40°C	0.52±0.06 Pa·s	0.54±0.02 Pa·s

Caloric Value	ASTM D240	22.95+0.85 MJ/kg	17.5±0.1 MJ/kg
Boiling Point	ASTM 7398	295±3.0°C	290±2.5°C
Melting Point	ASTM D87	20.8 ±1.7°C	17.8 ±0.92°C

TGA was used to observe the thermal degradation trend and provide quantitative measurements of the approximate composition (moisture, volatiles, fixed carbon, and minerals) of the crude and pure glycerol as captured in the temperature versus weight loss at four heating rates shown in Fig. 3. Contrary to the pure compound, crude glycerol consists of multiple peaks instead a single one. As these samples are oxidized, the crude resulted in three main DTG peaks and four thermal degradation stages. The first stage is the evaporation of methanol and moisture starting near 50°C to (138–156°C) comprising 10–12% weight loss. Pure glycerol, however, in this temperature range/ stage shows only 3% weight loss. The actual glycerol degradation takes place in the second stage comprising 70–70.8% weight loss for the crude and takes place in the temperature range 138–416°C. In comparison pure glycerol within this stage it shows nearly 97% weight loss extending from 135–161°C to 245–281°C temperature range. Degradation of the impurities occurs in the third stage for the crude that comprises 7–10% weight loss in the temperature range 336–417°C to 490-514°C. This compares to less than 0.9% for the pure taking place in the temperature range 244°C-700°C. The combustion of the remaining coke and ash for the crude occurs at the end in the 490-514°C to 700°C temperature range and comprises 5-7% weight loss. This stage does not exist for pure glycerol. The results of TG and DTG for both crude and pure glycerol are summarized in Table . Based on the thermographs, increasing the heating rate shifts the TG and DTG to higher degradation temperature while the overall trends remain unchanged. This is attributed to heat transfer limitation as lower heating rate results in larger instantaneous energy, and consequently longer time is required for the purge gas to reach equilibrium with the furnace temperature [28]. Furthermore, and within the same temperature range, a higher heating rate is associated with a shorter and insufficient reaction time that is compensated with higher temperature to do the decomposing.

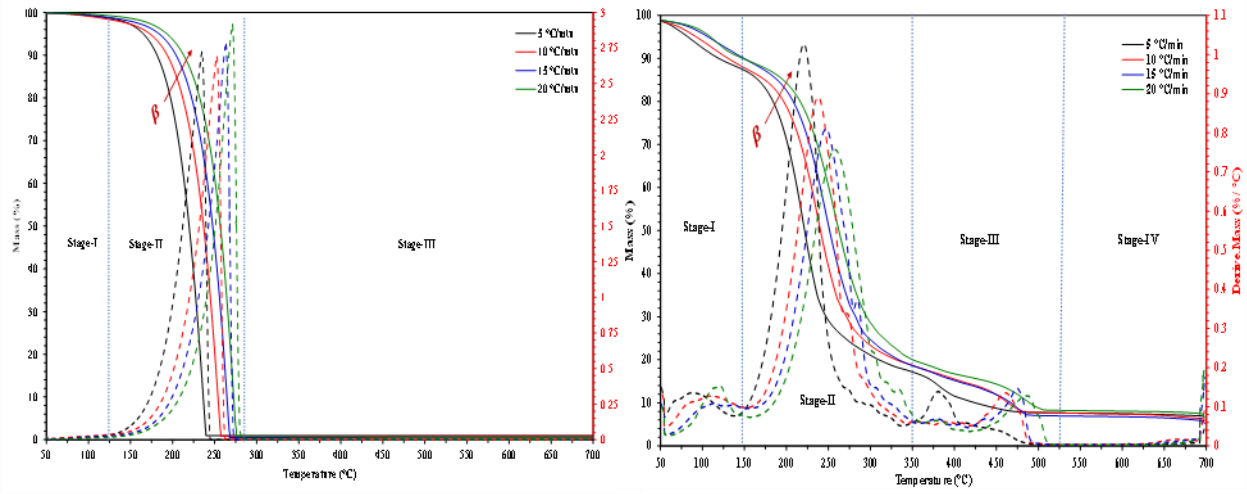

a **b**

Fig. 3: TG-DTG results at different heating rates (5, 10, 15, and 20°C min^{-1}) for (a) Pure and (b) Crude glycerol

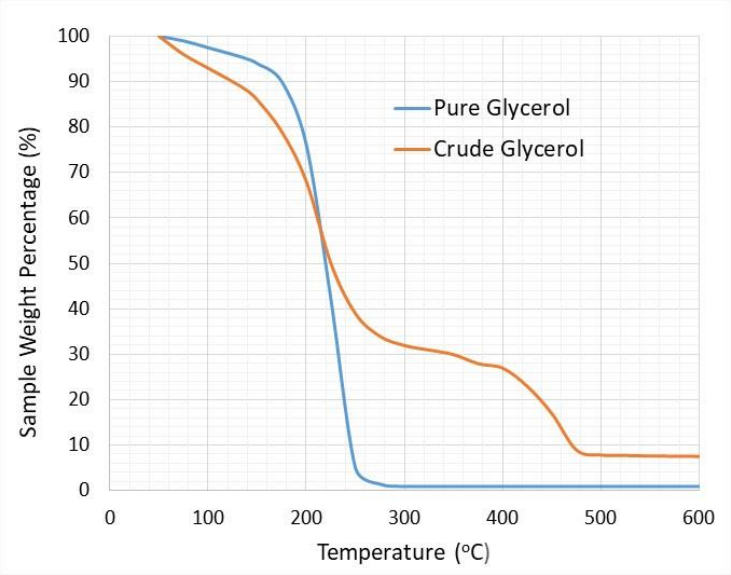

Fig. 4: TGA thermograph for the crude and pure glycerol at different heating rates

Usually, each step or event of weight loss is characterized with a specific surrogate of similar components that also correspond to temperature range. As can be seen in the average and superimposed Fig. 4 for both crude and pure glycerol, the pure is characterized with a single event weight loss, however, a mixture like the crude byproduct (mixture of 6 subcomponents at least) is a multi-event weight loss and the composition can be inferred according to the figure. While pure glycerol is considered as a single devolatilized component the crude consists of nearly 1.9±1.3% methanol, 4.6±2.6% moisture, 71.3±5.7% pure glycerol, 3.4±0.8% unreacted monoglyceride and di-glyceride, 13.4±1.6% triglyceride and nearly 5.3±0.5% minerals (catalyst). Different higher heating rate, which is typical in gasification, can push these percentages by a large margin as noticed earlier in Fig. 3.

Table 3: Summary of TGA and DTG characteristics for the crude and pure glycerol at different heating rate

Stage	TGA Characteristics	5°C/min	10°C/min	15°C/min	20°C/min
I Crude	T range [°C]	50–138.0	50–151.7	50–152.3	50–156.0
	Mass [%]	11.7	12.3	10.3	10.7
	T_{max} [°C]	87.5	107.7	113.2	120.7
	DTG_{max} [%/°C]	0.1	0.1	0.1	0.2
I Pure	T range [°C]	50–135.9	50–144.1	50–153.5	50–161.2
	Mass [%]	1.8	2.5	2.2	1.8
II Crude	T range [°C]	138.0–336.8	151.7–417.7	152.3–417.7	156.0–416.4
	Mass [%]	70.3	73.2	75.5	73.3
	T_{max} [°C]	220.6	237.7	247.0	257.5
	DTG_{max} [%/°C]	1.0	0.9	0.8	0.8
II Pure	T range [°C]	135.9–244.7	144.1–262.4	153.5–273.1	161.2–281.1
	Mass [%]	97.3	96.8	97.3	97.4
	T_{max} [°C]	234.9	252.4	263.1	271.1.0
	DTG_{max} [%/°C]	2.7	2.7	2.8	2.9
III Crude	T range [°C]	336.8–490.9	417.7–504.6	417.7–501.6	416.4–514.1
	Mass [%]	10.2	6.7	7.1	7.7
	T_{max} [°C]	380.7	460.7	374.5	486.3
	DTG_{max} [%/°C]	0.1	0.1	0.1	0.1
III Pure	T range [°C]	244.7–700	262.4–700	273.1–700	281.1–700
	Mass [%]	0.9	0.8	0.5	0.7

IV	T range [°C]	490.9–700	504.6–700	501.6–700	514.1–700
Crude	Mass [%]	7.8	7.7	7.0	8.3

The differences between crude and pure glycerol emphasize the difficulty in the refinement of the crude glycerol to compete with the abundant and low market price of pure glycerol. Instead, a proposition of performing thermo-chemical conversion of glycerol would not only eliminate the treatment process, but also lower the cost of the whole biodiesel transesterification reaction by producing another source of energy. Although the material to be dealt with is crude glycerol, as a start for the modeling of glycerol pyrolysis, the properties of pure glycerol are employed. This assumption is supported by the percentage of pure glycerol present in the byproduct which takes up to 60%. Hence, the density, boiling point, molecular and chemical formulas, etc. that are an input to the models belong to pure glycerol.

3.2 Low Fidelity Analysis

The model is used to obtain an idealistic performance of the gasification conversion of the glycerol. This idealistic thermo-conversion route is attempted under three conditions, namely pyrolysis or absence of the oxidizer and moderator, steam gasification or reforming, and combined steam and air gasification.

3.2.1 Glycerol Pyrolysis

Practically, glycerol pyrolysis is realized either by spraying/ injecting the liquid fuel in a hot (<900K), and preferably pressurized, inert atmosphere (i.e., N_2) environment. Alternatively, fast pyrolysis mode would work whereby the feedstock is subjected to several thousand-degree Kelvins per minute as in the case of plasma gasification. This would follow the gasification stoichiometry of **Error! Reference source not found.**.

The results under different values of temperature are depicted in Fig. 5. It is clear that at a higher pyrolysis temperature, higher syngas mole fractions were obtained which implies higher conversion and thereby higher cold gasification efficiency. The syngas fractions are the largest dominated by H_2 while the combustion species (H_2O and CO_2) are in decline as pyrolysis temperature increases. The overall pyrolysis reaction is an endothermic reaction and hence is more favored to the left based on Le Chatelier's principle. However, increasing the temperature would increase the reaction constant for the process and hence a compromise for temperature is needed to enable the reaction. This is seen in the attained plateau by the cold gasification efficiency with a maximum CGE of 38.64% reached at 1559 K. It is noted that the amount of heat added decreases as the temperatures increases. The evaluated value is used for the design of the pyrolysis reactor and to estimate its utility power load or its required heat as obtained from other sustainable resources, i.e. solar irradiation or industrial waste heat. Pyrolysis seems to give a good syngas yield; however, it requires a sealed reactor with no oxygen or steam influx. Additionally, high temperature glycerol pyrolysis requires a moderator such as steam, but not CO_2, denoting the gasification process more appropriately as reforming.

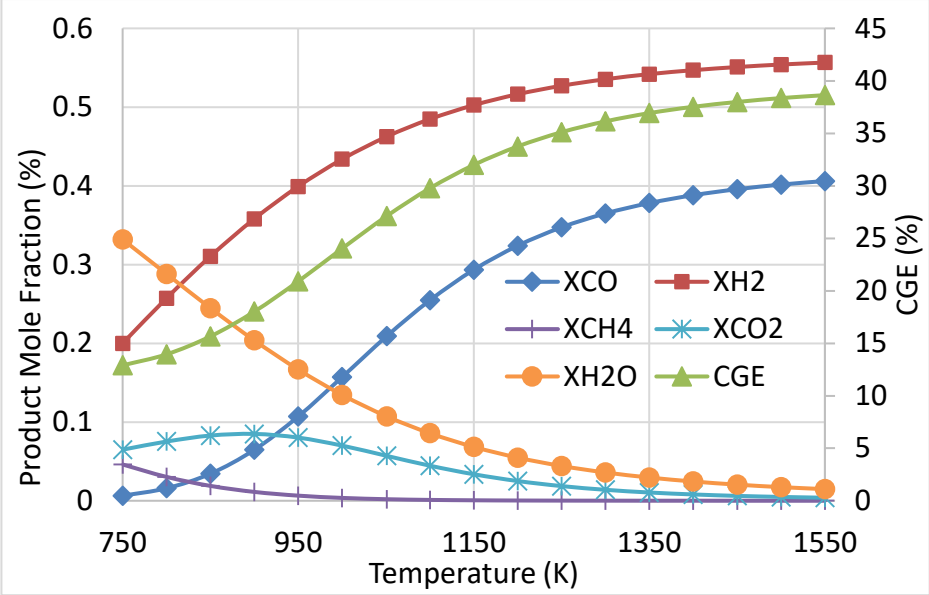

Fig. 5: Product mole fractions and the CGE of glycerol pyrolysis at different temperatures

3.2.2 Glycerol Steam Reforming

For the endothermic glycerol steam reforming, the overall reaction follows **Error! Reference source not found.**. However, practical experience shows that this equation is rather a two-step reaction. The first is the pyrolysis reaction that was explained earlier per **Error! Reference source not found.**, while the second is the water-gas shift in which the short-lived CO is consumed as per **Error! Reference source not found.**.

Stoichiometrically, one mole glycerol consumes three moles of water to proceed with the steam reforming, but higher (thrice as much) is recommended for the consumption of the CO and achieving a high H_2 yield. Therefore, the influence of the steam molar ratio and temperature is carried out and results are depicted in

Fig. 6 (a). It is done over sweeping values of H_2O molars, but extracted at 3, 6, and 9 H_2O moles per one mole of glycerol. The data is presented at different temperature values to facilitate the comparison. It is clearly observed that beyond stoichiometry, increasing steam molar produces more moles of H_2 while CO moles continue to diminish. This is attributed to the favorable conditions of the shift reaction that consumes the CO. It is also observed that at equal H_2O molar ratio the least moles of CO were obtained at the lowest temperature whereas the highest H_2 is produced at near 1,000K.

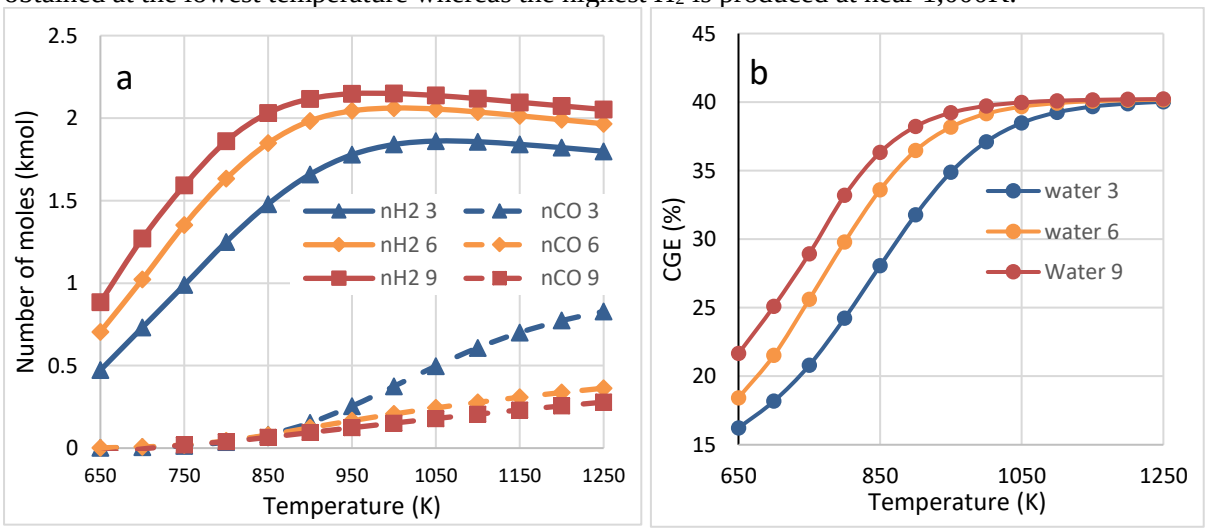

Fig. 6: Left: (a) Syngas number of moles at different H_2O:GL molar ratios (3, 6 and 9) and temperatures. Right: (b) CGE at different H_2O:GL molar ratios (3, 6 and 9) and temperatures

Since it is not very clear how the effect of temperature and molar ratio is on syngas mole production, the evaluation of CGE can set things in perspective as depicted in

Fig. 6 (b). At high temperatures of 1250K, CGE is highest (40%) with no variation happening at increased molar ratios. Enhanced CGE values are attained at elevated temperatures. At lower temperatures (< 1,250K), CGE is higher at larger H_2O: glycerol ratios. Thus, gasification efficiency for glycerol is increased at higher temperatures and H_2O molar ratios. Hence, these analyses suggest that it is better to carry out glycerol steam reforming at elevated temperatures and steam molar ratio far from equilibrium analysis point of view. However, higher temperatures require more power and increasing water: glycerol molar results in a diluted product that requires refined separation. The development of the suitable conditions for glycerol conversion reactor requires a settlement between the obtained results from the low fidelity systematic analysis, considering the most effective and feasible implementation.

3.3 High Fidelity Modelling of Glycerol Conversion

In an attempt to obtain a more accurate comprehension of glycerol pyrolysis, a high-fidelity computational fluid dynamics (CFD) model is developed. The temperature profile along the reactor axis for a wall temperature was set at 1173.15 K as displayed in Fig. 7. The discrete phase model (DPM) mass source of glycerol is also shown in the same figure. The results illustrate that the glycerol droplets convert to syngas when the temperature within the reactor reaches the devolatilization temperature of glycerol according to chemical kinetics. External heat supply was included through the wall of the gasifier in order to enhance the endothermic reactions such as devolatilization and water gas shift reactions. The contour profile of the temperature and centreline plot is described in Fig. 8. The temperature profile shows a gradient from the inlet up until it attains a peak value of 1164K at around 9cm along the axis. The temperature near the entry at the center line was lower due to the heating of the relatively cold feedstock towards their endothermic devolatilization. Although the vaporization temperature of the glycerol is 341 K, a higher temperature is important in order to ensure complete pyrolysis [12, 29]. Further along the center line, the temperature was elevated due to the subsequent exothermic homogeneous reactions of the released volatiles. Thereafter, the temperature was maintained at the maximum with little fluctuations. Similar temperature behavior can be found elsewhere [30, 31].

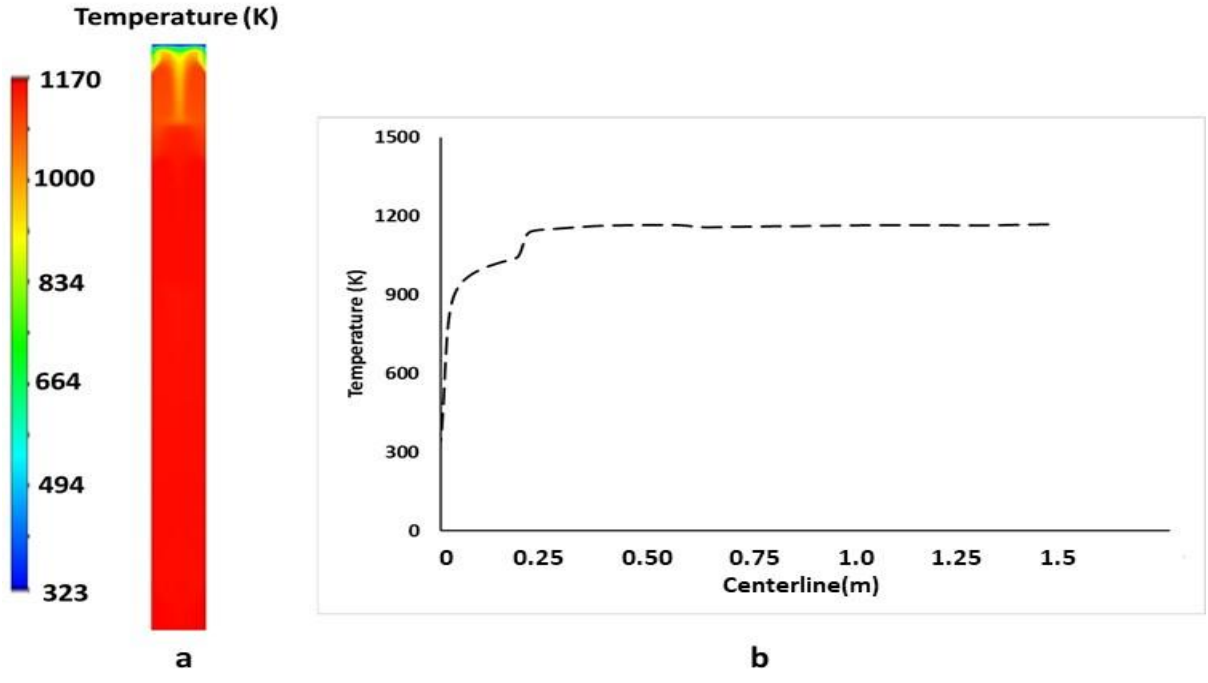

Fig. 7: (a) Temperature contour plot inside the drop tube gasifier (b) Centerline plot of the temperature during the gasification of glycerol

As soon as the glycerol is sprayed into the inlet, it devolatilizes and subsequently converts to syngas. The presence of char and tar was neglected in the numerical model due to their absence in actual experiments. This characteristic has been reported in the experimental study of Guo et al. [32], as well as in the work of Chakinala et al. [33]. The main product gases obtained were CO and H_2, but CO_2 and H_2O were observed along the drop tube gasifier. The production of CO_2 and H_2O with syngas is consistent with several reports of the experimental gasification of different feedstocks [34, 35]. The center line progression of the gaseous species showed that the H_2 and CO showed a general increasing trend in the gasifier. However, the mass fraction of the CO showed reductions towards the exit, which can be associated with the backflow of oxidants at the outlet. In contrast, the CO_2 and H_2O showed a decreasing trend in the reactor.

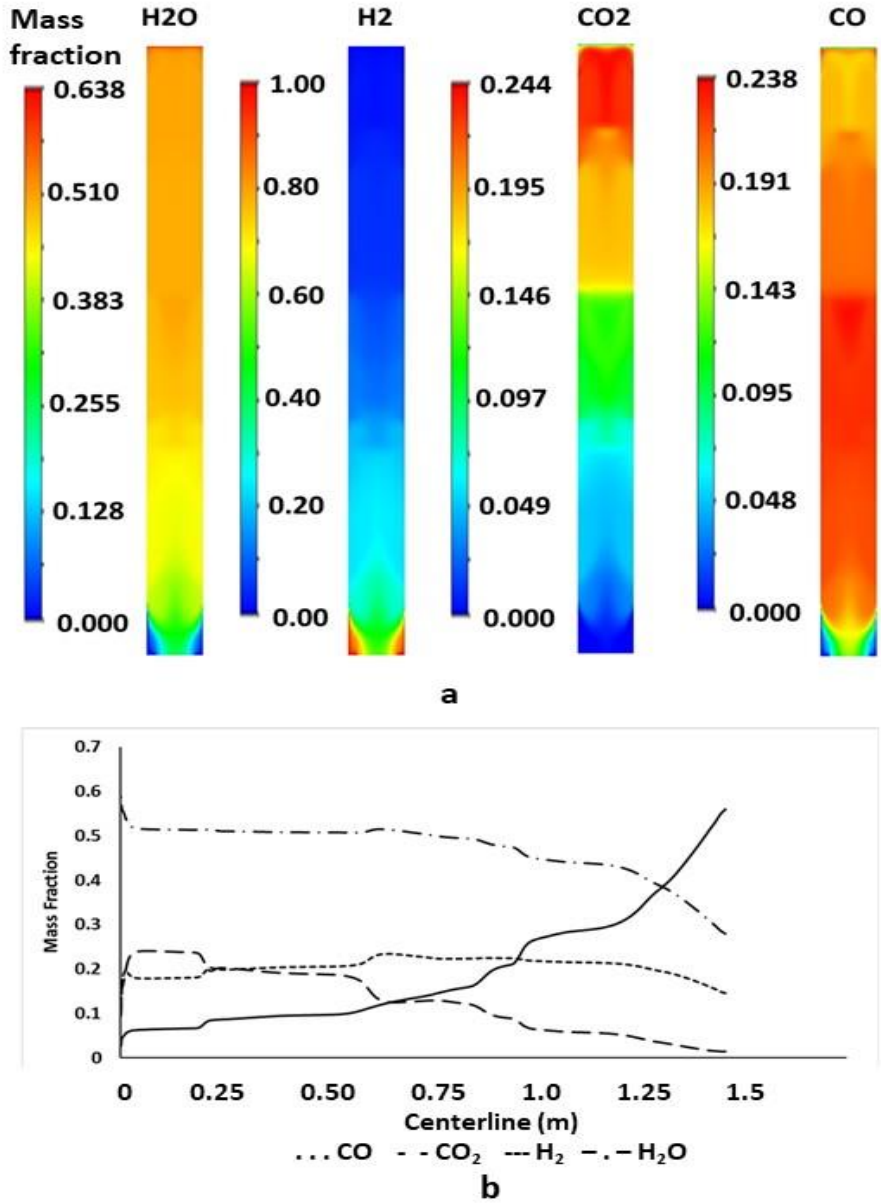

Fig. 8: (a) Species distribution contour plot for H_2O, H_2, CO_2 and CO inside the drop tube gasifier (b) Centerline plot of the gas species during the gasification of glycerol

3.4 Economic Feasibility Assessment

The feasibility of the gasification at molar ratios of 3, 6 and 9 for water:glycerol was assessed at 650-1250K. Generally, the price of the produced H_2 increased until it reaches peak values of \$7.4, \$8.2 and \$8.6 for molar ratios 3,6 and 9 at 950K, respectively. Likewise, the monetary value of the CO increased with rising gasification temperature. In addition, the quantities and price of H_2 rose but the value of CO reduced with increasing molar ratios. Based on the cost estimations for the CO and H_2, the monetary value of the syngas was determined. As expected, the price of the syngas increases with increasing temperature. The increment in temperature enables the enhanced rates of the endothermic gasification reactions. Similar observation was noted in the works of Dou et al [36] and Sarafraz et al [37]. Moreover, at temperatures below 970K, the amount and price of syngas produced increased with rising molar ratio. This is consistent with the fact that higher molar ratios produced more H_2, which has relatively more significant cost compared to CO. However, after 970K, the reverse trend can be observed with lower molar ratios producing better syngas values. Also, the prices of the generated syngas at molar ratios of 6 and 9 were very close in this region.

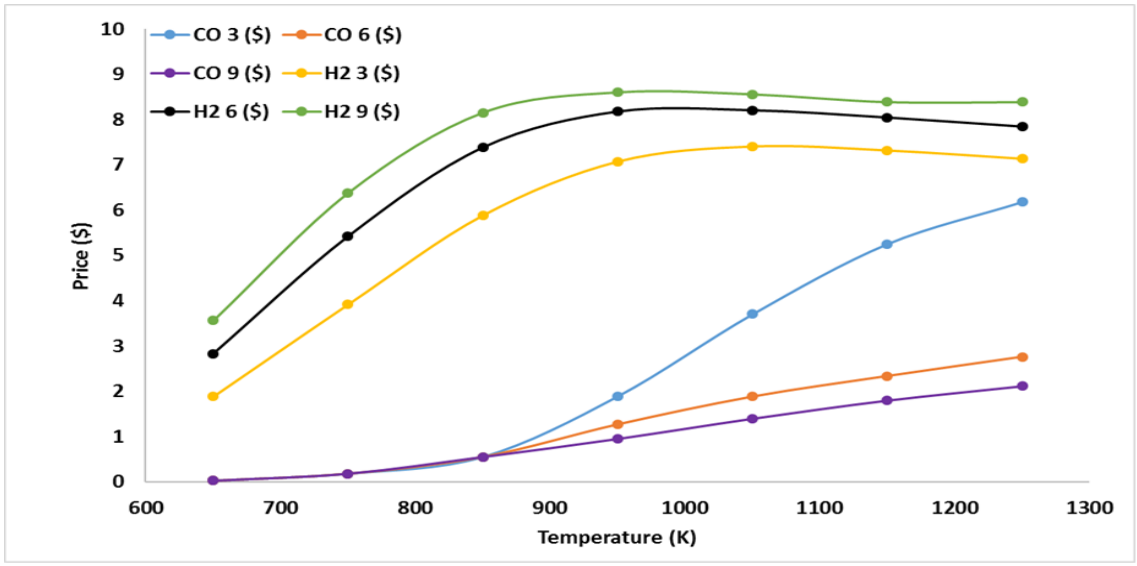

a

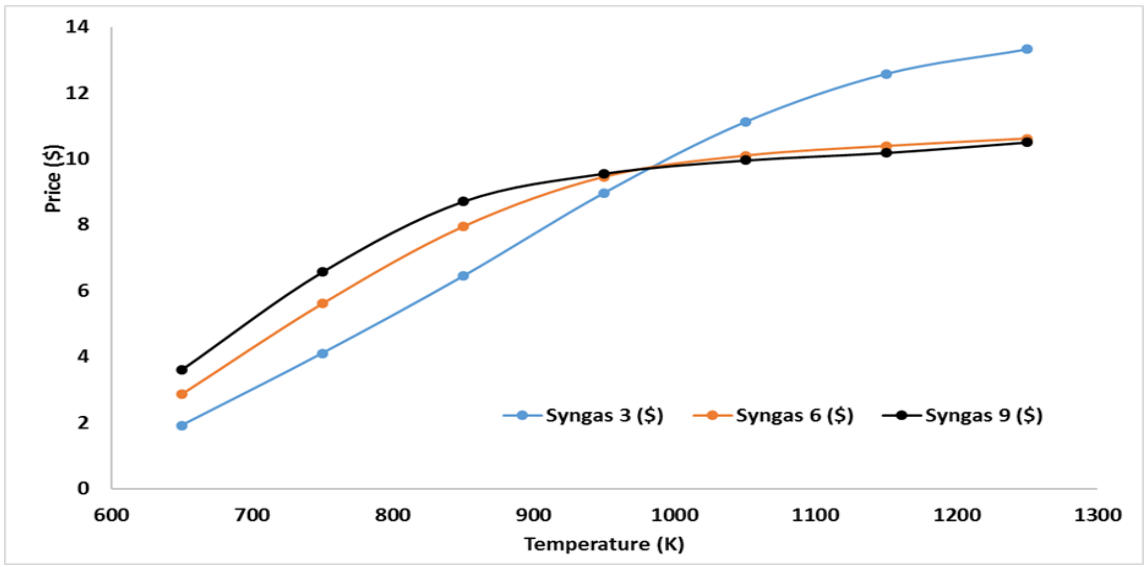

b

Fig. 10: Comparative assessment of the price: (a) carbon monoxide and hydrogen at molar ratios 3, 6 and 9, (b) syngas at molar ratios 3, 6 and 9

Subsequently, the net gain ($) was estimated by taking into account the cost of attaining the wall temperatures 650-1250K. The results show that lower temperatures are not favorable economically for the gasification of glycerol. This can be attributed to the reduced syngas yield at lower temperatures. For the molar ratio of 3, there was net profit at temperatures above 950K. However, it is not economically feasible under all temperature conditions for molar ratios of 6 and 9. These results provide insights into the economic optimization of glycerol gasification process based on the impact of molar ratios of oxidizer and feedstock.

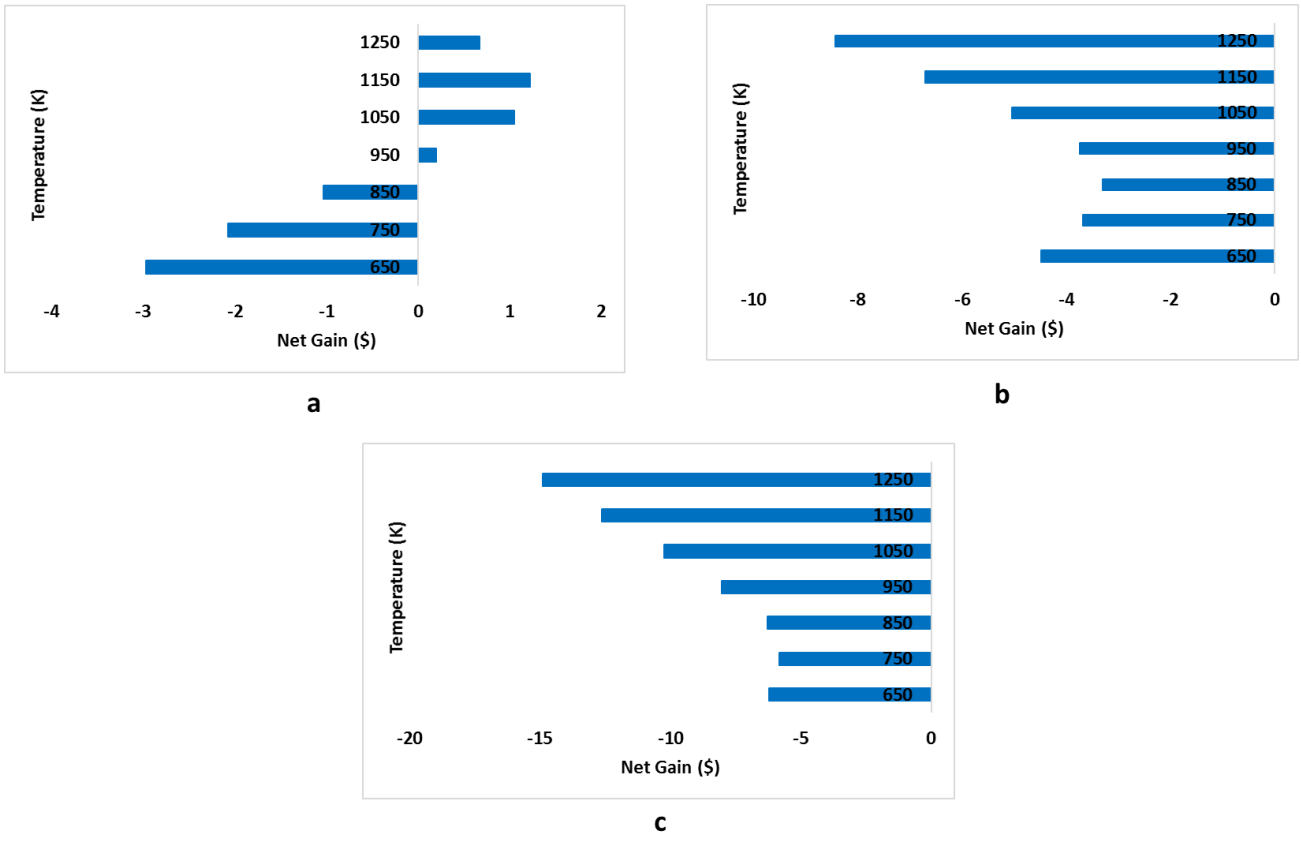

Fig. 11: Comparative assessment of the net gain ($) (a) molar ratio of 3 (b) molar ratio of 6 **c** molar ratio of 9

4. Conclusions

In this study, the technical feasibility of gasification of crude glycerol was assessed at two levels, equilibrium modeling which was conducted under ideal conditions, and high-fidelity reactive flow modeling in a tubular reactor. Results revealed that elevated steam ratio is required for the gasification of glycerol to reach high conversion efficiency (99%) and an acceptable cold gasification efficiency of 40%. Although this value is far from the conventional coal gasification that hovers around 60%, it suggests that gasification of crude glycerol can be accepted as a short to long term solution of the expected flood of glycerol generated by the biodiesel transesterification industry before becoming a waste burden. The contrast between pure and crude glycerol proves the difficulty associated with the byproduct refinement. Zero-dimensional systematic analysis of glycerol thermochemical conversion shows the effectiveness of steam reforming and pyrolysis over the partial combustion (gasification) of glycerol. Initial results obtained from high fidelity modeling indicate that glycerol converts to syngas at moderate temperatures (627°C) which is in line with literature conversion temperatures.

Credit author statement

All authors contributed to the study conception and design. **Tala El Samad:** Original draft preparation, Methodology, Writing- Reviewing and Editing, and Data analysis & interpretation. **Idowu Adeyemi:** Conceptualization, Methodology, Software and writing & Investigation. **Chaouki Ghenai:** The conceptualization, Original draft preparation and Data analysis & interpretation. **Isam Janajreh:** The conceptualization, Original draft preparation and Data analysis & interpretation, Methodology, Supervision, Software, Validation, Writing- Reviewing and Editing

Acknowledgements

The sponsorship received from Khalifa University of Science and Technology under the Grant number [RC2-2018-009] is highly acknowledged.

Funding

This work was supported by Khalifa University of Science and Technology (Grant number [RC2-2018-009]). Author Isam Janajreh has received this research support grant.

Declaration of Competing Interest

The authors declare that they have no known competing financial interests or personal relationships that could have appeared to influence the work reported in this paper.

References

[1] R. W. M. Pott, C. J. Howe, and J. S. Dennis, "The purification of crude glycerol derived from biodiesel manufacture and its use as a substrate by Rhodopseudomonas palustris to produce hydrogen," *Bioresour Technol*, vol. 152, pp. 464–470, Jan. 2014, doi: 10.1016/J.BIORTECH.2013.10.094.

[2] R. Ciriminna, C. della Pina, M. Rossi, and M. Pagliaro, "Understanding the glycerol market," *European Journal of Lipid Science and Technology*, vol. 116, no. 10, pp. 1432–1439, Oct. 2014, doi: 10.1002/EJLT.201400229.

[3] P. Vadthya, A. Kumari, C. Sumana, and S. Sridhar, "Electrodialysis aided desalination of crude glycerol in the production of biodiesel from oil feed stock," *Desalination*, vol. 362, pp. 133–140, Apr. 2015, doi: 10.1016/J.DESAL.2015.02.001.

[4] F. D. Pitt, A. M. Domingos, and A. A. C. Barros, "Purification of residual glycerol recovered from biodiesel production," *S Afr J Chem Eng*, vol. 29, pp. 42–51, Jul. 2019, doi: 10.1016/J.SAJCE.2019.06.001.

[5] S. J. Yoon, Y. M. Yun, M. W. Seo, Y. K. Kim, H. W. Ra, and J. G. Lee, "Hydrogen and syngas production from glycerol through microwave plasma gasification," *Int J Hydrogen Energy*, vol. 38, no. 34, pp. 14559–14567, Nov. 2013, doi: 10.1016/J.IJHYDENE.2013.09.001.

[6] R. Mangayil, M. Karp, and V. Santala, "Bioconversion of crude glycerol from biodiesel production to hydrogen," *Int J Hydrogen Energy*, vol. 37, no. 17, pp. 12198–12204, Sep. 2012, doi: 10.1016/J.IJHYDENE.2012.06.010.

[7] B. Dou, V. Dupont, P. T. Williams, H. Chen, and Y. Ding, "Thermogravimetric kinetics of crude glycerol," *Bioresour Technol*, vol. 100, no. 9, pp. 2613–2620, May 2009, doi: 10.1016/J.BIORTECH.2008.11.037.

[8] M. Gupta and N. Kumar, "Scope and opportunities of using glycerol as an energy source," *Renewable and Sustainable Energy Reviews*, vol. 16, no. 7, pp. 4551–4556, Sep. 2012, doi: 10.1016/J.RSER.2012.04.001.

[9] M. S. Macedo, M. A. Soria, and L. M. Madeira, "Process intensification for hydrogen production through glycerol steam reforming," *Renewable and Sustainable Energy Reviews*, vol. 146, p. 111151, Aug. 2021, doi: 10.1016/J.RSER.2021.111151.

[10] B. F. Tapah, R. C. D. Santos, and G. A. Leeke, "Processing of glycerol under sub and supercritical water conditions," *Renew Energy*, vol. 62, pp. 353–361, Feb. 2014, doi: 10.1016/J.RENENE.2013.07.027.

[11] Y. S. Stein, M. J. Antal, and M. Jones, "A study of the gas-phase pyrolysis of glycerol," *J Anal*

Appl Pyrolysis, vol. 4, no. 4, pp. 283–296, Mar. 1983, doi: 10.1016/0165-2370(83)80003-5.
[12] T. Valliyappan, N. N. Bakhshi, and A. K. Dalai, "Pyrolysis of glycerol for the production of hydrogen or syn gas," *Bioresour Technol*, vol. 99, no. 10, pp. 4476–4483, Jul. 2008, doi: 10.1016/J.BIORTECH.2007.08.069.
[13] S. Adhikari *et al.*, "A thermodynamic analysis of hydrogen production by steam reforming of glycerol," *Int J Hydrogen Energy*, vol. 32, no. 14, pp. 2875–2880, Sep. 2007, doi: 10.1016/J.IJHYDENE.2007.03.023.
[14] T. Hirai, N. O. Ikenaga, T. Miyake, and T. Suzuki, "Production of Hydrogen by Steam Reforming of Glycerin on Ruthenium Catalyst," *Energy and Fuels*, vol. 19, no. 4, pp. 1761–1762, Jul. 2005, doi: 10.1021/EF050121Q.
[15] B. Zhang, X. Tang, Y. Li, Y. Xu, and W. Shen, "Hydrogen production from steam reforming of ethanol and glycerol over ceria-supported metal catalysts," *Int J Hydrogen Energy*, vol. 32, no. 13, pp. 2367–2373, Sep. 2007, doi: 10.1016/J.IJHYDENE.2006.11.003.
[16] S. Adhikari, S. D. Fernando, and A. Haryanto, "Hydrogen production from glycerol: An update," *Energy Convers Manag*, vol. 50, no. 10, pp. 2600–2604, Oct. 2009, doi: 10.1016/J.ENCONMAN.2009.06.011.
[17] U.S. Department of Energy, "Clean Cities Alternative Fuel Price Report," 2022.
[18] S. N. Gebremariam and J. M. Marchetti, "Economics of biodiesel production: Review," *Energy Convers Manag*, vol. 168, pp. 74–84, Jul. 2018, doi: 10.1016/j.enconman.2018.05.002.
[19] C. A. G. Quispe, C. J. R. Coronado, and J. A. Carvalho, "Glycerol: Production, consumption, prices, characterization and new trends in combustion," *Renewable and Sustainable Energy Reviews*, vol. 27, pp. 475–493, 2013, doi: 10.1016/J.RSER.2013.06.017.
[20] M. Ripoll and L. Betancor, "Opportunities for the valorization of industrial glycerol via biotransformations," *Curr Opin Green Sustain Chem*, vol. 28, p. 100430, Apr. 2021, doi: 10.1016/J.COGSC.2020.100430.
[21] I. Janajreh, M. Noorul Hussain, T. el Samad, and F. Ataya, "CONTINUOUS SONO-CHEMICAL REACTORS AND METHODS OF USING THE SAME," Dec. 2019.
[22] M. N. Hussain and I. Janajreh, "Acousto-chemical analysis in multi-transducer sonochemical reactors for biodiesel production," *Ultrason Sonochem*, vol. 40, pp. 184–193, Jan. 2018, doi: 10.1016/J.ULTSONCH.2017.07.009.
[23] I. Janajreh, T. ElSamad, and M. Noorul Hussain, "Intensification of transesterification via sonication numerical simulation and sensitivity study," *Appl Energy*, vol. 185, pp. 2151–2159, Jan. 2017, doi: 10.1016/J.APENERGY.2016.02.002.
[24] S. Shabbar and I. Janajreh, "Thermodynamic equilibrium analysis of coal gasification using Gibbs energy minimization method," *Energy Convers Manag*, vol. 65, pp. 755–763, Jan. 2013, doi: 10.1016/J.ENCONMAN.2012.02.032.
[25] I. Talab, Z. Al-Nahari, R. Qudaih, and I. Janajreh, "Numerical Modeling of Coal Tire-Shred Co-Gasifcation," *Jordan Journal of Mechanical and Industrial Engineering*, vol. 4, no. 1, pp. 155–162, Jan. 2010.
[26] X. Lü, Y. Sun, T. Lu, F. Bai, and M. Viljanen, "An efficient and general analytical approach to modelling pyrolysis kinetics of oil shale," *Fuel*, vol. 135, pp. 182–187, Nov. 2014, doi: 10.1016/J.FUEL.2014.06.009.
[27] S. Shabbar and I. Janajreh, "Thermodynamic equilibrium analysis of coal gasification using Gibbs energy minimization method," *Energy Convers Manag*, vol. 65, pp. 755–763, Jan. 2013, doi: 10.1016/J.ENCONMAN.2012.02.032.
[28] L. Mazzoni, M. Almazrouei, C. Ghenai, and I. Janajreh, "A comparison of energy recovery from MSW through plasma gasification and entrained flow gasification," *Energy Procedia*, vol. 142, pp. 3480–3485, Dec. 2017, doi: 10.1016/j.egypro.2017.12.233.
[29] Y. Fernández, A. Arenillas, M. A. Díez, J. J. Pis, and J. A. Menéndez, "Pyrolysis of glycerol over activated carbons for syngas production," *Journal of Analytical and Applied Pyrolysis*, vol. 84, no. 2, pp. 145–150, Mar. 2009, doi: 10.1016/j.jaap.2009.01.004.
[30] J. Mularski and N. Modliński, "Impact of Chemistry–Turbulence Interaction Modeling Approach on the CFD Simulations of Entrained Flow Coal Gasification," *Energies*, vol. 13, no. 23, p. 6467, Dec. 2020, doi: 10.3390/en13236467.
[31] I. Adeyemi, I. Janajreh, T. Arink, and C. Ghenai, "Gasification behavior of coal and woody

biomass: Validation and parametrical study," *Applied Energy*, vol. 185, pp. 1007–1018, Jan. 2017, doi: 10.1016/j.apenergy.2016.05.119.

[32] S. Guo, L. Guo, J. Yin, and H. Jin, "Supercritical water gasification of glycerol: Intermediates and kinetics," *The Journal of Supercritical Fluids*, vol. 78, pp. 95–102, Jun. 2013, doi: 10.1016/j.supflu.2013.03.025.

[33] A. G. Chakinala, D. W. F. (Wim) Brilman, W. P. M. van Swaaij, and S. R. A. Kersten, "Catalytic and Non-catalytic Supercritical Water Gasification of Microalgae and Glycerol," *Ind. Eng. Chem. Res.*, vol. 49, no. 3, pp. 1113–1122, Feb. 2010, doi: 10.1021/ie9008293.

[34] T. Valliyappan, D. Ferdous, N. N. Bakhshi, and A. K. Dalai, "Production of Hydrogen and Syngas via Steam Gasification of Glycerol in a Fixed-Bed Reactor," *Top Catal*, vol. 49, no. 1–2, pp. 59–67, Jul. 2008, doi: 10.1007/s11244-008-9062-7.

[35] G. Salierno, F. Marinelli, B. Likozar, N. Ghavami, and C. De Blasio, "Supercritical Water Gasification of glycerol: Continuous reactor kinetics and transport phenomena modeling," *International Journal of Heat and Mass Transfer*, vol. 183, p. 122200, Feb. 2022, doi: 10.1016/j.ijheatmasstransfer.2021.122200.

[36] Dou, B., Song, Y., Wang, C., Chen, H., & Xu, Y. (2014). Hydrogen production from catalytic steam reforming of biodiesel byproduct glycerol: Issues and challenges. Renewable and Sustainable Energy Reviews, 30, 950-960.

[37] Sarafraz, M. M., Safaei, M. R., Jafarian, M., Goodarzi, M., & Arjomandi, M. (2019). High Quality Syngas production with supercritical biomass gasification integrated with a water–gas shift reactor. Energies, 12(13), 2591.